PRRL-76-CR-43

ERDA/JPL/954465-76/2
Distribution Category UC-63

SILICON SHEET GROWTH BY THE INVERTED STEPANOV TECHNIQUE

K. M. Kim, G. W. Cullen, S. Berkman,
and A. E. Bell
RCA Laboratories
Princeton, New Jersey 08540

QUARTERLY REPORT NO. 2
(also ANNUAL REPORT)

September 1976

NOTICE
This report was prepared as an account of work sponsored by the United States Government. Neither the United States nor the United States Energy Research and Development Administration, nor any of their employees, nor any of their contractors, subcontractors, or their employees, makes any warranty, express or implied, or assumes any legal liability or responsibility for the accuracy, completeness or usefulness of any information, apparatus, product or process disclosed, or represents that its use would not infringe privately owned rights.

This work was performed for the Jet Propulsion Laboratory, California Institute of Technology, under NASA Contract NAS7-100 for the U. S. Energy Research and Development Administration, Division of Solar Energy.

The JPL Low-Cost Silicon Solar Array Project is funded by ERDA and forms part of the ERDA Photovoltaic Conversion Program to initiate a major effort toward the development of low-cost solar arrays.

Prepared Under Contract No. 954465 For
JET PROPULSION LABORATORY
CALIFORNIA INSTITUTE OF TECHNOLOGY
Pasadena, California 91103

DISTRIBUTION OF THIS DOCUMENT IS UNLIMITED

DISCLAIMER

This report was prepared as an account of work sponsored by an agency of the United States Government. Neither the United States Government nor any agency thereof, nor any of their employees, makes any warranty, express or implied, or assumes any legal liability or responsibility for the accuracy, completeness, or usefulness of any information, apparatus, product, or process disclosed, or represents that its use would not infringe privately owned rights. Reference herein to any specific commercial product, process, or service by trade name, trademark, manufacturer, or otherwise does not necessarily constitute or imply its endorsement, recommendation, or favoring by the United States Government or any agency thereof. The views and opinions of authors expressed herein do not necessarily state or reflect those of the United States Government or any agency thereof.

DISCLAIMER

Portions of this document may be illegible in electronic image products. Images are produced from the best available original document.

UNCLASSIFIED

SECURITY CLASSIFICATION OF THIS PAGE (When Data Entered)

REPORT DOCUMENTATION PAGE

READ INSTRUCTIONS BEFORE COMPLETING FORM

Field	Entry
1. REPORT NUMBER	
2. GOVT ACCESSION NO.	
3. RECIPIENT'S CATALOG NUMBER	
4. TITLE (and Subtitle)	SILICON SHEET GROWTH BY THE INVERTED STEPANOV TECHNIQUE
5. TYPE OF REPORT & PERIOD COVERED	Quarterly No. 2 (also Annual Report) (7/16/76 to 9/30/76)
6. PERFORMING ORG. REPORT NUMBER	PRRL-76-CR-43
7. AUTHOR(s)	K. M. Kim, G. W. Cullen, S. Berkman, and A. E. Bell
8. CONTRACT OR GRANT NUMBER(s)	954465
9. PERFORMING ORGANIZATION NAME AND ADDRESS	RCA Laboratories Princeton, New Jersey 08540
10. PROGRAM ELEMENT, PROJECT, TASK AREA & WORK UNIT NUMBERS	
11. CONTROLLING OFFICE NAME AND ADDRESS	Jet Propulsion Laboratory California Institute of Technology Pasadena, California 91103
12. REPORT DATE	September 1976
13. NUMBER OF PAGES	42
14. MONITORING AGENCY NAME & ADDRESS (if different from Controlling Office)	
15. SECURITY CLASS. (of this report)	Unclassified
15a. DECLASSIFICATION/DOWNGRADING SCHEDULE	N/A

16. DISTRIBUTION STATEMENT (of this Report)

Distribution category UC-63

17. DISTRIBUTION STATEMENT (of the abstract entered in Block 20, if different from Report)

18. SUPPLEMENTARY NOTES

This work was performed for the Jet Propulsion Laboratory, California Institute of Technology, under NASA Contract NAS7-100 for the U. S. Energy Research and Development Administration, Division of Solar Energy.

The JPL Low-Cost Silicon Solar Array Project is funded by ERDA and forms part of the ERDA Photovoltaic Conversion Program to initiate a major effort toward the development of low-cost solar arrays.

19. KEY WORDS (Continue on reverse side if necessary and identify by block number)

Silicon ribbon growth
Inverted Stepanov Technique
SiO_2 die
Pyrolytic BN die

20. ABSTRACT (Continue on reverse side if necessary and identify by block number)

IST silicon ribbon growth has been pursued with SiO_2 die, and efforts have been made to improve the stability of the ribbon growth. By grounding both the susceptor and the metal shield of the thermocouple, it has been possible to measure a more realistic temperature distribution accurately without any rf interferences. Various thermal modifiers are being designed and tested to achieve a satisfactory

DD FORM 1473 1 JAN 73

UNCLASSIFIED

SECURITY CLASSIFICATION OF THIS PAGE (When Data Entered)

20.

thermal gradient for the stable ribbon growth. The growth apparatus has been modified to supplement the gravity feed with gas pressure. The stability of the ribbon growth has improved significantly with a small pressure differential (∿1 mm Hg). Using our one-dimensional computer simulation of the growing ribbon, which now includes the term which corresponds to convective heat transport within the ribbon, we have examined the influence of the growth velocity on the height of the molten zone and the thermal characteristics of the growing ribbon. Results are presented for both high (1300 K) and low (300 K) ambient temperature, and the effect of varying the die temperature and the ribbon thickness is also examined. Cost estimates of the IST silicon ribbon growth are initiated.

PREFACE

This Quarterly Report No. 2, prepared by RCA Laboratories, Princeton, NJ 08540, describes work performed under Contract No. 954465 in the Process and Applied Materials Research Laboratory, P. Rappaport, Director, and in the Communications Research Laboratory, K. H. Powers, Director. G. W. Cullen is the Group Head and the Project Supervisor. K. M. Kim is the Project Scientist. Others who participated in the research and writing of this report are S. Berkman, A. E. Bell (thermal analysis), H. E. Temple, R. E. Novak, and J. C. Toner (cost analysis).

The JPL Project Monitor is K. M. Koliwad.

TABLE OF CONTENTS

Section		Page
I.	SUMMARY	1
II.	INTRODUCTION	2
III.	PROGRESS AND TECHNICAL DISCUSSION	6
	A. IST Silicon Ribbon Growth Experiments with SiO_2 Die	6
	1. Silicon Ribbon Growth Instabilities with SiO_2 Die	6
	2. Application of Pressure Differential for Ribbon Growth Stability	7
	3. Measurement of Thermal Gradients and Thermal Trimming	9
	B. Thermal Analysis of the IST Ribbon Growth	13
	1. Mathematical and Computational Aspects of the Model	13
	2. Results of One Dimensional Model for Growing Silicon Ribbon (STEP2C)	15
	C. Cost Estimates of IST Silicon Ribbon Production	24
IV.	CONCLUSIONS AND FUTURE PLANS	28
REFERENCES		29
APPENDIX A - New Technology		31
APPENDIX B - Program Plan		32
APPENDIX C - Manhours and Costs		33

LIST OF ILLUSTRATIONS

Figure | Page

1. Schematic drawing of silicon ribbon growth by IST 3
2. Schematic of the IST silicon ribbon growth arrangement provided with a pressure differential 8
3. Calibration curve of the pressure differential vs argon flow rate 9
4. Photograph of a short (0.05 cm) SiO_2 capillary slot which has been used in the ribbon growth with pressure differential. (Mag. 10X). 10
5. Schematic of the temperature measurement configuration. Note that the junction is exposed to accurately measure the temperature distribution. The susceptor and the sheath of the thermocouple are grounded 10
6. The horizontal temperature distribution at the edge of the SiO_2 die slot at three different temperatures. Thermocouple was touching the edge of the fused silica die 11
7. The vertical temperature distribution along the midpoint of the SiO_2 die slot. A thermal trimmer of 3-mm-thick pyrolytic graphite plate is positioned underneath the graphite susceptor 12
8. Effect of convective heat transport on the temperature profile of the growing ribbon. Ribbon 0.0375 x 1.0 cm, 3.0 cm long. Die temperature 1690 K, ambient temperature 300 K, growth velocity 0.11 cm/s 15
9. Temperature profile in vicinity of molten zone as a function of growth velocity. Ribbon 0.0375 x 1.0 cm, 3.0 cm long. Die temperature 1690 K, ambient temperature 300 K 17
10. Zone height (normalized to ribbon thickness) as a function of growth velocity taken from the data shown in Fig. 9 17
11. Temperature profile in vicinity of molten zone as a function of growth velocity. Ribbon 0.0375 x 1.0 cm, 3.0 cm long. Die temperature 1690 K, ambient temperature 1300 K 19
12. Temperature profile in vicinity of molten zone as a function of growth velocity. Ribbon 0.0375 x 1.0 cm, 3.0 cm long. Die temperature 1685 K, ambient temperature 1300 K 20
13. Zone height (normalized to ribbon thickness) as a function of growth velocity taken from data shown in Figs. 11 and 12 20
14. Temperature profile in vicinity of molten zone as a function of growth velocity. Ribbon 0.0187 x 1.0 cm, 3.0 cm long. Die temperature 1190 K, ambient temperature 300 K 23
15. Zone height (normalized to ribbon thickness) as a function of growth velocity taken from data shown in Fig. 14 23

LIST OF TABLES

Table Page

1. Effect of the Convective Transport Term on the Total Power Dissipation and its Distribution Between the Various Modes of Dissipation 16
2. Influence of Growth Velocity on the Thermal Characteristics of Growing Ribbon for 300 K Ambient and 1690 K Die Temperature 18
3. Influence of Growth Velocity on Thermal Characteristics of a Growing Ribbon for 1300 K Ambient With Die Temperatures of 1690 K and 1685 K, respectively 22
4. Influence of Growth Velocity on Thermal Characteristics of 0.0187- x 1.0-cm Growing Ribbon for 300 K Ambient and 1690 K Die Temperature 25

SECTION I

SUMMARY

Measurement of the temperatures to profile the horizontal and vertical thermal gradients has been pursued. By grounding both the susceptor and the metal shield of the thermocouple it has been possible to use an unsheathed, bare thermocouple to measure a more realistic temperature distribution. The thermal gradients with thermal trimmers, such as the L-shaped graphite and pyrolytic graphite plate, are not satisfactory. Further effort is being made to achieve a satisfactory thermal gradient by design of a suitable thermal modifier configuration.

The growth apparatus has been modified to supplement the gravity feed with gas pressure. The susceptor/SiO_2 die assembly was positioned on top of a quartz pedestal with a controlled gas leak. The flow of argon through the leak supplies a pressure differential across the melt. In a preliminary ribbon growth experiment, with a pressure differential of about 1-mm Hg, ribbon growth was stable. The ribbon did not spread to a width greater than $\sim$0.3 cm wide, apparently due to the unsatisfactory isotherm.

We have completed our computer program, STEP2C, which simulates the thermal profile along the growth direction of a moving silicon ribbon, including terms corresponding to both the liberation of latent heat at the freezing boundary of the molten zone and the convective heat transport within the moving ribbon. Our results show that for given ribbon geometry, die temperature, and ambient condition, as the growth velocity is increased the height of the molten zone increases, becoming ever more rapid as the velocity approaches and exceeds a critical growth velocity.

The critical growth velocity depends on the particular ambient condition and die temperature as well as the ribbon geometry, but is greatest for low ambient temperatures and die temperatures which approach the melting point most closely; some increase in growth velocity is also achieved by reducing the thickness of the growth ribbon.

The cost estimates of the IST silicon ribbon production are in progress and will be described in the next report.

SECTION II

INTRODUCTION

The overall objective of the Inverted Stepanov program is to maintain the potential for economical silicon sheet growth characteristic of the EFG (or CAST) process [1,2] while minimizing the interference with crystal growth which results from the reaction between the die and the molten silicon. Wetted carbon dies are commonly employed in the EFG process. The dissolution of the carbon by silicon, and the subsequent incorporation of silicon carbide into the growing crystal, has been identified as one important source of degradation in the crystalline quality of the ribbon silicon grown using the wetted carbon die. It is anticipated that the incorporation into the silicon of reaction products between the silicon and the die material can be minimized by use of a non-wetted (or at least less wetted) die material.

The silicon ribbon growth method under investigation is based on the inversion of the Stepanov configuration [3,4] which uses "non-wetting" dies of high contact angle (near to 90°). In this growth configuration, which is represented schematically in Fig. 1, the silicon ribbon crystal grows downward. The hydrostatic pressure in the melt enhances the feeding of the melt and thus compensates partially for the lack of capillary feeding which is inherent in the "non-wetting" die. In this configuration, hydrostatic pressure may also readily be supplemented by gas pressure, if desired.

Silicon ribbons up to 2 cm wide have been grown by the IST process using pyrolytic BN dies which have a contact angle of 110°. Satisfactory thermal gradients were realized by positioning a flat BN plate die inside a rectangular

---

1. J. C. Schwartz, T. Surek, and B. Chalmers, J. Electronic Mat. 4, 255 (1975); H. E. Bates, F. H. Cocks, and A. I. Mlavsky, "Thick Film Silicon Growth Techniques," NAS7-100/JPL-953365, First Quarterly Progress Report, July 1972.
2. T. F. Ciszek, Mat. Res. Bull. 7, 731 (1972).
3. A. V. Stepanov et al., Bull. Acad. Sci. USSR, Phys. Series 33, 1826 (1969).
4. P. C. Goundry and J. C. Boatman, "Investigation of Single Crystal Si Ribbon," AFAL-TR-66-312, Part I, Sept. 1966, and Part II, Oct. 1967.

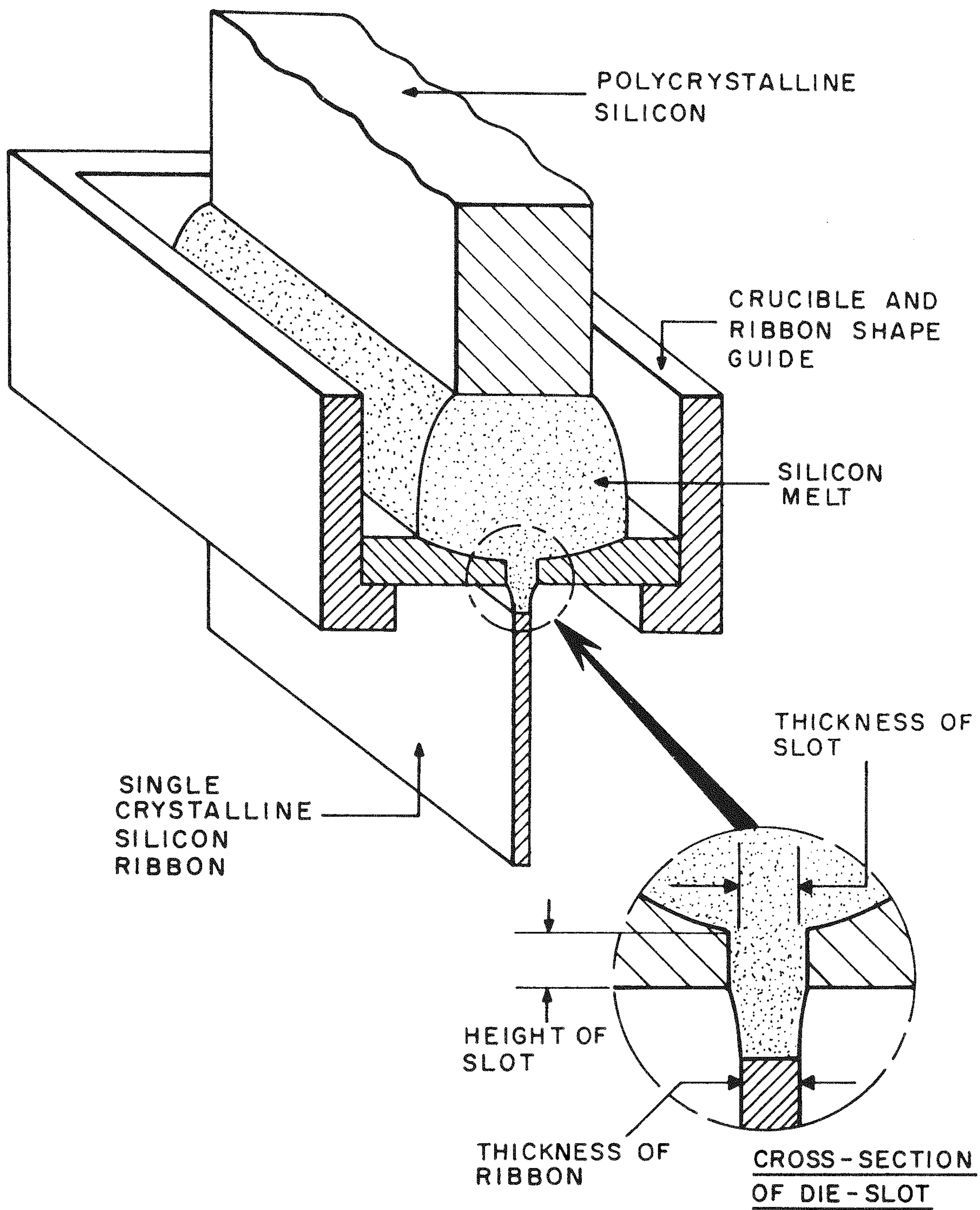

Figure 1. Schematic drawing of silicon ribbon growth by IST.

susceptor on top of a pyrolytic graphite plate (a thermal trimmer) (see Quarterly Report No. 1 [5]). Since the silicon ribbon was too heavily doped with boron ($\sim 8 \times 10^{19}/cm^3$) to be applied effectively in solar cell fabrication, growth conditions to improve the crystalline quality were not pursued.

In this reporting period, the use of a fused silica die in the "V" shaped susceptor/die configuration [5] has been emphasized. While the SiO_2 die offers the possibility of avoiding the incorporation of both the impurities and the inclusions which act either as active dopants in the silicon or degradate the crystalline quality, a disadvantage in the use of this material is that it is soft at the melting point of silicon. To provide mechanical support, the "V" shaped configuration was developed. This configuration also facilitates the machining and construction of the die package, with the result that modifications can be done more rapidly and many more experimental growth runs can be carried out within a given time period. While the "V" shaped geometry was originally designed under the conditions where the feed through the slot was assisted by hydrostatic pressure only, this configuration is equally useful when the hydrostatic head is supplemented with gas pressure. We have decided, during the last report period, that greater flexibility is realized with the application of gas pressure across the melt, and therefore this feature has been incorporated into the IST process. The application of a pressure differential across the melt suppresses the oscillatory vertical motion in the melt apparently induced by the erratic wetting behavior of the liquid silicon with the fused silica.

Coupling of the rf field into the "V" shaped configuration is considerably different than into the "rectangular" shaped susceptor/die arrangement. Therefore, the thermal gradients must be re-established. The objective is to combine favorable thermal conditions characteristic of the "rectangular" die with the favorable mechanical properties of the "V" shaped die. Efforts are being made to achieve satisfactory thermal conditions in the "V" configuration by adding thermal trimmers and measuring the temperature distributions.

Since the success of this ribbon growth process is so critically dependent on the thermal configuration, a detailed theoretical thermal analysis of the

---

5. K. M. Kim et al., "Silicon Sheet Growth by the Inverted Stepanov Technique," Quarterly Report No. 1, ERDA/JPL/954465-76/1, prepared under Contract No. 954465 for Jet Propulsion Laboratory, June 1976.

method has been continued. This analysis not only provides important guidance for design of the apparatus, but also brings to light what may prove to be some fundamental limitations on the growth rate. It is anticipated that an appreciation of these limitations will lead to the configuration providing the maximum growth rate possible with this process.

To date, we had assumed that the costs of the IST method would be the same, within the capability of projecting such costs, as the EFG method. On the other hand it has become evident, on the examination of cost projections provided for a number of the growth methods, that the numbers developed are highly dependent on the basic approach used. Therefore, we have initiated an effort to develop cost estimates employing procedures in which assumptions are minimized, and the details of the specific process are emphasized.

SECTION III

PROGRESS AND TECHNICAL DISCUSSION

A. IST SILICON RIBBON GROWTH EXPERIMENTS WITH SiO_2 DIE

1. Silicon Ribbon Growth Instabilities with SiO_2 Die

Silicon ribbon growth with the fused silica die in the inverted Stepanov configuration has been pursued in this reporting period. The "V" shaped crucible-die configuration was employed which has been described in detail in the last quarterly report [5]. During the initial part of this reporting period, the capillary slot was 0.05 x 2.5 cm wide, and the capillary height was 0.3 cm; then a shorter capillary slot of 0.05 cm was used to improve the mechanical rigidity of the slot during the ribbon growth (see Fig. 4 in the following subsection). Silicon seeds of (110) $[\bar{1}12]$ or (111) $[\bar{2}11]$ orientation have been used. Typically, the seeds are 0.03 x 1.0 to 1.5 cm wide and about 5 cm long.

The silica die slot is readily filled with the liquid silicon to the lower edge of the die. The melt inside the slot can be seeded and ribbon growth initiated after thermal equilibration of the system. The meniscus height is then adjusted to approximately 0.02 to 0.07 cm by adjusting the heat input. Low ribbon pull rates have been used to date, i.e., from 3 to 10 cm/h. After ∿0.2 cm of ribbon growth, growth instabilities usually set in. The ribbon either freezes to the die or separates from the melt, as has been reported previously.

To date, adjustment of the thermal gradients by using different thermal trimmers and beveling the inner capillary edge to 45° have not alleviated the growth instabilities.

Unsatisfactory thermal gradients can be one of the major factors which lead to the growth instabilities. Therefore, we measured the thermal gradients with various thermal trimmers, as discussed in subsection III.A.3 below. Efforts are in progress to select thermal trimmers which would provide satisfactory horizontal and vertical temperature gradients.

The other important factor which results in ribbon growth instabilities is the erratic wetting behavior of the liquid silicon with the fused silica. It has been observed that the silicon melt in the crucible and the die slot is in constant motion in the vertical direction. This is not observed in the pyrolytic BN crucible-die positioned in the same configuration. The formation and evolution of silicon monoxide apparently cause the erratic wetting behavior and the mechanical vibration in the melt.

Such erratic wetting behavior and mechanical vibration of the liquid silicon inside the narrow die slot affect the stability of the meniscus shape in the IST silicon ribbon growth. Similar erratic wetting behavior has been reported in the preliminary EFG silicon growth employing fused silica capillary [1].

2. Application of Pressure Differential for the Stability of Ribbon Growth

A pressure differential was applied to bring the meniscus out of the die slot and to stabilize the ribbon growth. The hydrostatic pressure in the melt in the IST configuration supplies some pressure differential across the melt. By increasing the melt height (currently 1.0 cm), the pressure differential can be increased. However, since the present simple, efficient crucible-die design must be changed to accommodate a higher melt height, we have adopted an alternative method to supply the auxiliary pressure differential by means of constricted gas flow.

Figure 2 is a schematic of the IST silicon ribbon growth arrangement used to apply a pressure differential. A pyrolytic graphite plate with the "a-b" plane perpendicular to the ribbon growth axis was attached to the lower side of the susceptor/SiO_2 die assembly and positioned on top of a fused silica pedestal; this is provided with eight holes of 0.15-cm diameter which can be plugged with fused silica rods, if necessary, to increase the pressure differential. Due to the argon flow from the upper space in the chamber through the leaks in the pedestal, a pressure differential was established. Figure 3 shows the pressure differential vs the flow rate of argon. The pressure differential was measured by a U-type manometer filled with a low vapor pressure oil. At a flow rate of 5 ft^3/h, a pressure difference of 1.5 mm of oil (density = 0.96 g/cm^3) was measured. At 2-mm pressure difference, the meniscus (not seeded) started to protrude outside the slot edge.

The thickness of the ribbon was about 0.1 cm, while the die slot was 0.05 cm thick; this is due to the fact that the liquid silicon came out of

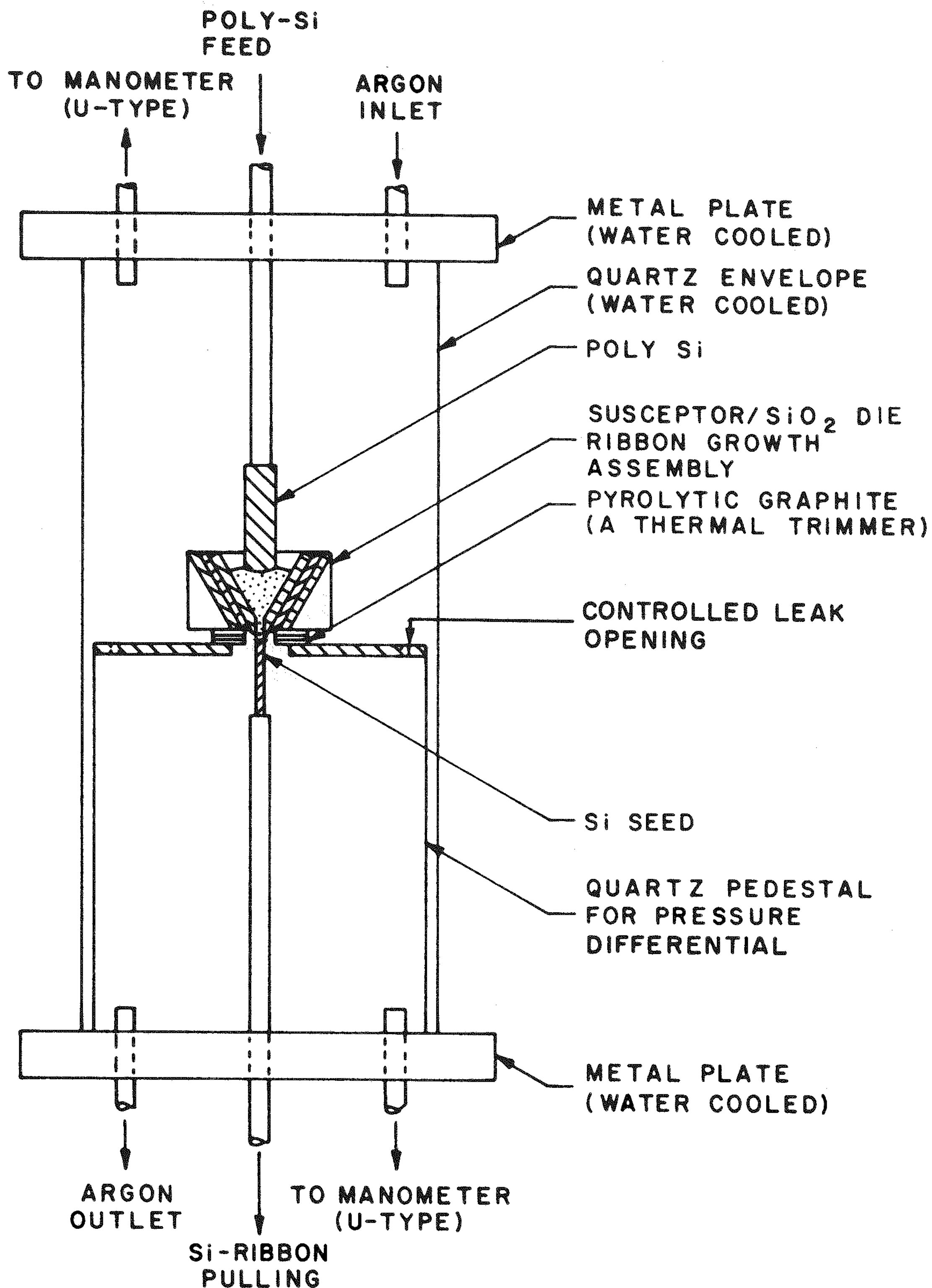

Figure 2. Schematic of the IST silicon ribbon growth arrangement provided with a pressure differential.

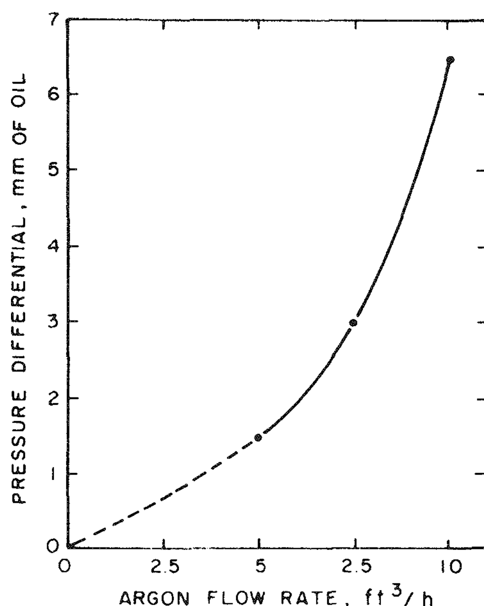

Figure 3. Calibration curve of the pressure differential vs argon flow rate.

the slot under the pressure differential and spread slightly to the outer edges of the die.

Figure 4 shows a fused silica die with the shorter capillary height (0.05 cm) which is being used in the ribbon growth with the pressure differential. The short die with flat edge is mechanically more rigid than the long die with triangular edge which has been employed previously [5].

3. Measurement of the Thermal Gradient and Thermal Trimming

The thermal gradients in the "V" shaped susceptor-die configuration have been measured. The current ribbon growth apparatus, Model 1, was modified so that the thermocouple could be moved within the system in order to measure the horizontal and vertical temperature gradients continuously at high temperatures. By grounding the susceptor and the metal shield of the thermocouple it was possible to use an unshielded thermocouple and to measure more realistic temperature distributions. Two kinds of thermocouples of fine gauge wires were used: Chromel/Alumel of 0.02-cm diameter and Pt-13%Rh/Pt of 0.025-cm diameter. Figure 5 is a schematic of the temperature measurement arrangement with a thermal trimmer. To simulate the growth thermal conditions, a fused silica die with a "V" shaped graphite insert (1 cm high, 4.1 cm long) was positioned inside the susceptor.

satisfactory isotherms realized with the rectangular susceptor with flat pyrolytic BN die and PG plate thermal trimmer, the PG plate in the new "V" shaped growth configuration must be heated more effectively by the rf field. Efforts are being made to pump more heat laterally into the PG plate to achieve a better isotherm and to decrease the vertical thermal gradient to prevent the SiO deposition at the top of the seed.

B. THERMAL ANALYSIS OF THE IST RIBBON GROWTH

1. Mathematical and Computational Aspects of the Model

During the past quarter we have continued to develop our one-dimensional computer simulation of the thermal profile along the silicon ribbon. We have completed the formulation of a second computer program, STEP2C, which computes the thermal profile along the growth direction of a growing silicon ribbon, and, in particular, we have applied this model to examine the height of the molten zone as a function of growth velocity for a variety of ambient temperatures, die temperatures, and ribbon thickness.

The differential equation which describes the diffusion of heat in a ribbon which moves with some finite velocity, V-cm/s, relative to the grid of meshpoints upon which the temperature profile is computed is given by

$$\frac{d}{dx}\left[\frac{KdT}{dx}\right] = \frac{2(w+t)}{wt}\left[\underbrace{\sigma\varepsilon\,(T^4 - T_o^{\,4})}_{\text{radiative loss}} + \underbrace{G\,(T - T_o)}_{\text{convective loss}}\right] + \underbrace{VC\,\frac{dT}{dx}}_{\text{convective transport term}} \qquad (1)$$

where

K is the thermal conductivity, $w/cm^2/°/cm$

w is the ribbon width, cm

t is the ribbon thickness, cm

σ is Stefan's constant, $w/cm^2/K^4$

ε is the emissivity of silicon

T_o is the ambient temperature, K

G is the convective heat transfer coefficient, $w/cm^2/K$

V is the growth velocity, cm/s

C is the volume specific heat of silicon, $joules/cm^3$

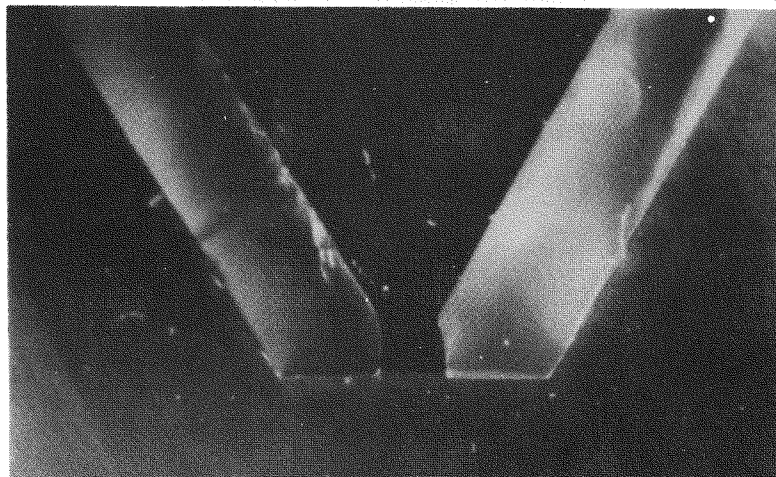

Figure 4. Photograph of a short (0.05 cm) SiO_2 capillary slot which has been used in the ribbon growth with pressure differential (Mag. 10X).

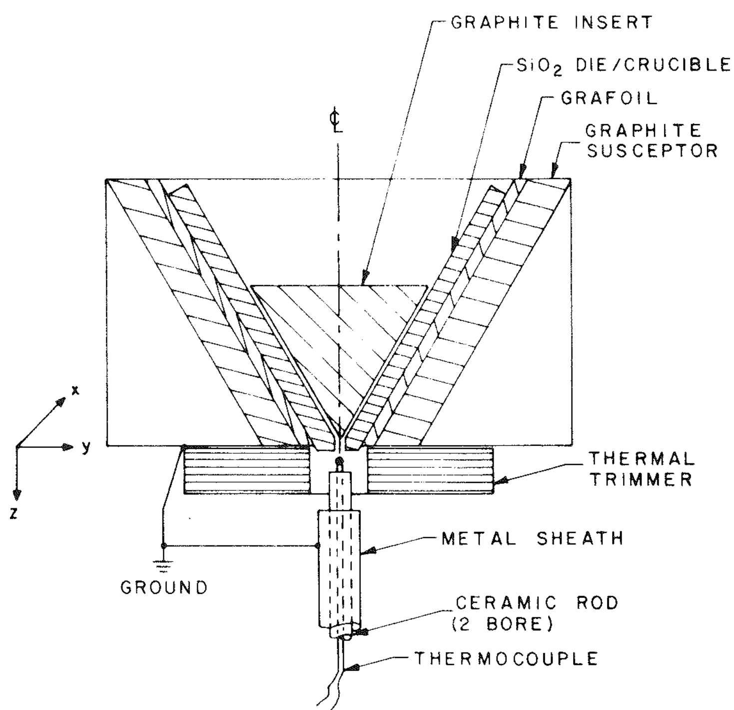

Figure 5. Schematic of the temperature measurement configuration. Note that the junction is exposed to accurately measure the temperature distribution. The susceptor and the sheath of the thermocouple are grounded.

Figure 6 shows the horizontal temperature profile as measured by the Chromel/Alumel thermocouple at three temperatures, i.e., 1038°, 118°, and 1207°C at the midpoint of the die edge. The thermocouple was touching the edge of the fused silica die. A pyrolytic graphite (PG) plate (5.1 x 2.0 x 2.3 cm thick) was used as the thermal trimmer; the high conductivity "a-b" plane was

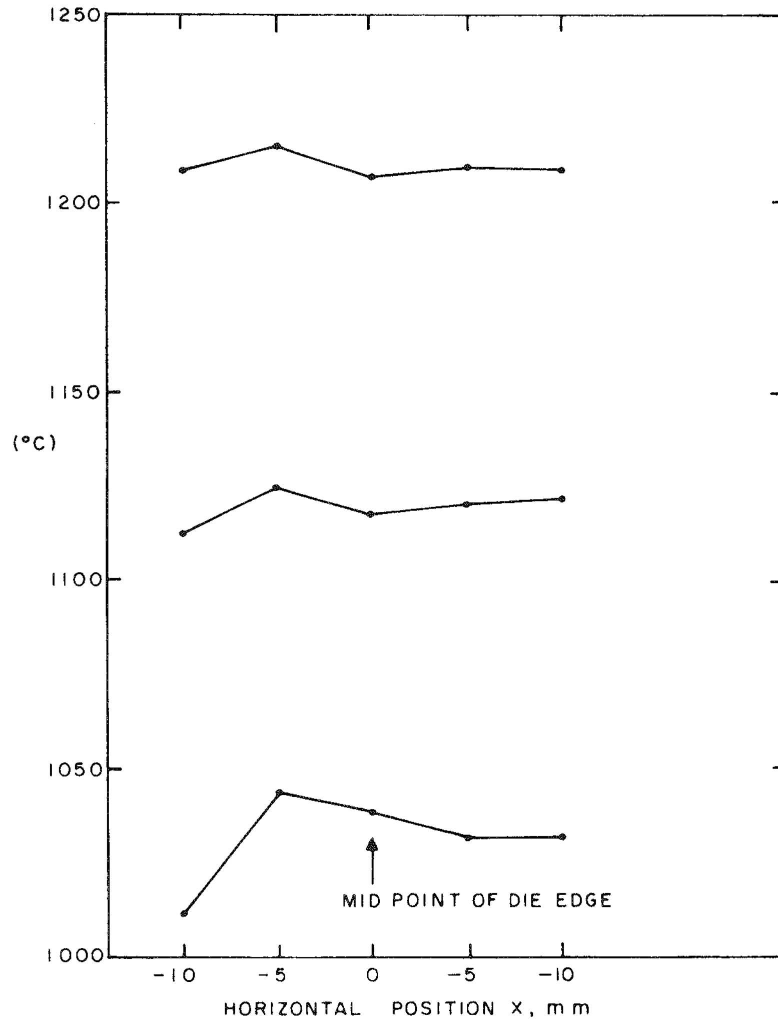

Figure 6. The horizontal temperature distribution at the edge of the SiO_2 die slot at three different temperatures. Thermocouple was touching the edge of the fused silica die.

positioned perpendicular to the vertical axis. The vertical temperature gradient along the midpoint at 1188°C is reproduced in Fig. 7. The temperature at the midpoint of the horizontal temperature profile is lower than along

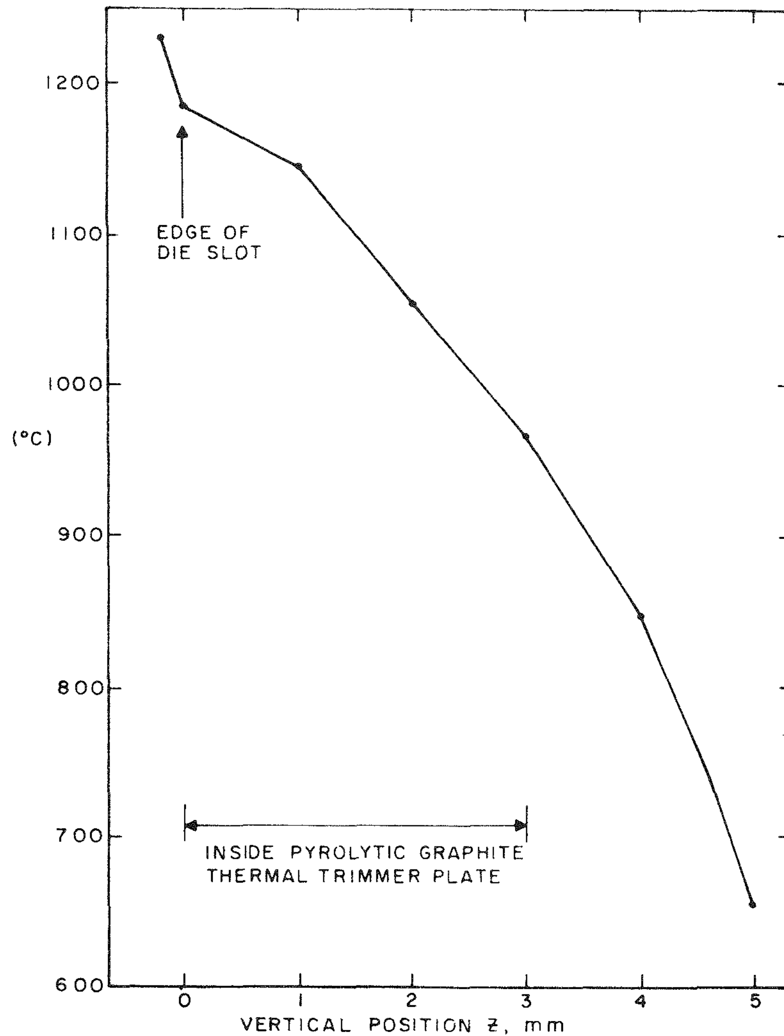

Figure 7. The vertical temperature distribution along the midpoint of the SiO_2 die slot. A thermal trimmer of 3-mm-thick pyrolytic graphite plate is positioned underneath the graphite susceptor.

both sides of the slot; a similar profile was observed with a L-shaped graphite thermal trimmer. Such a horizontal temperature profile has proven to be unfavorable for the ribbon growth. Ideally, the temperature near the midpoint should be slightly higher than the edges in order to offset the high heat loss during seeding and ribbon growth.

It is of interest to note that inside the 3-mm-thick pyrolytic graphite trimmer the vertical temperature gradient decreased almost linearly (Fig. 7); this implies that the PG plate was not coupling significantly to the rf field, but was heated through the conduction from the susceptor. To simulate the

Equation (1) differs from that of the stationary ribbon by the addition of the convective heat transfer term $VC \frac{dT}{dx}$ which represents the flow of heat along the mesh due to the translation of the hot silicon ribbon. Equation (1) was solved iteratively using the Gauss-Seidel procedure with accelerated relaxation, and the liberation of the latent heat of fusion at the freezing boundary of the molten zone was taken into account in the following manner. On each successive iteration, the temperature profile along the mesh was examined to determine the location of the freezing boundary and the index of the meshpoint which was closest to this boundary position. A quantity of heat just equal to $\dot{Q}_F$, the rate of liberation of latent heat, was then 'injected' into this meshpoint during the next iteration of the computation. $\dot{Q}_F$ depends only on the growth velocity and the cross-sectional area of the ribbon and is easily calculated from

$$\dot{Q}_F = V\,wt\,L \tag{2}$$

where L is the latent heat of fusion in joules/cm^3 for silicon.

The height of the molten zone is generally a very small fraction of the total length of the ribbon and in order to have sufficient spatial resolution to monitor the extent of the molten zone, several thousand meshpoints would be required. To avoid this tedious (and expensive) computation we have arranged for a variable meshpoint density along the grid. In the neighborhood of the molten zone where high resolution is required, the meshpoint spacing is chosen to be about 10% of the ribbon thickness, whereas in regions remote from the zone the meshpoint spacing is expanded to about 50% of the ribbon thickness. In this way the number of meshpoints is limited to be between 100 and 200.

In order to check the computed temperature profile we continue to evoke the principal of conservation of energy and compare the heat input to the ribbon with the total power dissipated to the ambient and, by conduction, to the clamp. Typically, with the variable meshpoint density we converge to a residual energy imbalance of 3% or less.

2. Results of One-Dimensional Model for Growing Silicon Ribbon (STEP2C)

To illustrate the effect of the convective heat transport term on the temperature profile, we computed the profile for a 3.0-cm-long, 1.0- x 0.0375-cm ribbon growing with a velocity of 0.11 cm/s in a 300 K ambient, both with and without the inclusion of the convective term. The results are shown in Fig. 8 and we see that where the convective transport term is included, there is a general elevation of the temperature profile along the ribbon to dissipate the additional heat input arising from convective transport

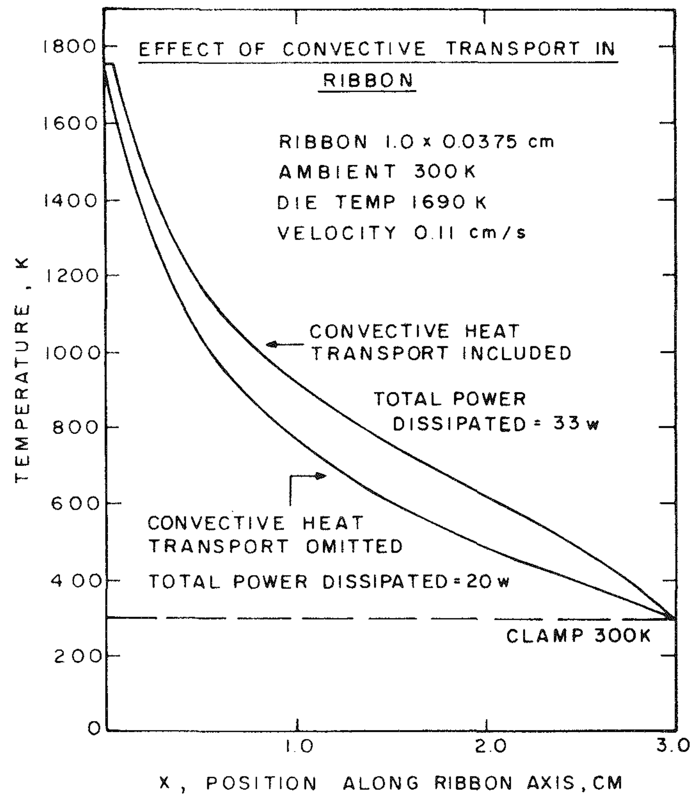

Figure 8. Effect of convective heat transport on the temperature profile of the growing ribbon. Ribbon 0.0375 x 1.0 cm, 3.0 cm long. Die temperature 1690 K, ambient temperature 300 K, growth velocity 0.11 cm/s.

from the die. The net convective heat input to the ribbon is given by

$$P_c = CV\,(T_D - T_{CL}')\;w\;t \qquad (3)$$

where T_D = die temperature, K

T_{CL} = clamp temperature, K

P_c is equal to 11.6 W in the case shown in Fig. 8. The total power dissipated in each case shown in Fig. 8 and the distribution by mode of dissipation are shown in Table 1.

TABLE 1. EFFECT OF THE CONVECTIVE TRANSPORT TERM ON THE TOTAL POWER DISSIPATION AND ITS DISTRIBUTION BETWEEN THE VARIOUS MODES OF DISSIPATION

Parameter	No convective transport (W)	Convective transport included (W)
Total power dissipated	19.7	33.3
Radiation loss	15.88	22.64
Convection loss	2.44	3.50
Clamp conduction loss	1.38	4.29
Clamp convective loss	0.00	2.86

In Fig. 9 we show the temperature profile in the neighborhood of the molten zone as a function of the ribbon growth velocity. In all cases the ribbon geometry (0.0375 x 1.0 cm, 3.0 cm long), die temperature (1690 K), and ambient temperature (300 K) remain unchanged and only the growth velocity is varied. In Fig. 10 we plot the molten zone height directly as a function of the growth velocity and we see an initially slow rate of increase of zone height which becomes ever more rapid as the growth velocity approaches and exceeds about 0.1 cm/s (2.36 in./min). Above this velocity the zone height rapidly approaches a value of twice the ribbon thickness, suggesting that the geometry of the growing ribbon may change, or, if the molten zone is sufficiently unstable at this point, separation of the ribbon from the die top may occur. In Table 2 we see that as the growth velocity is increased toward the critical value, both the latent heat and net convective heat input increase and the heat conducted from the die reduces to only about 10% of its value for a stationary ribbon. The total power dissipated from the ribbon also

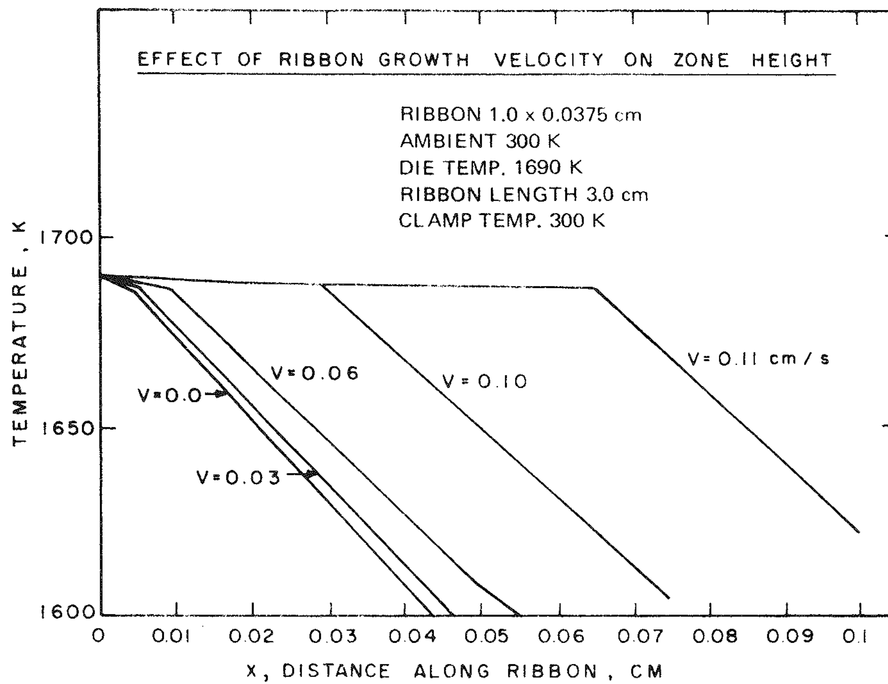

Figure 9. Temperature profile in vicinity of molten zone as a function of growth velocity. Ribbon 0.0375 x 1.0 cm, 3.0 cm long. Die temperature 1690 K, ambient temperature 300 K.

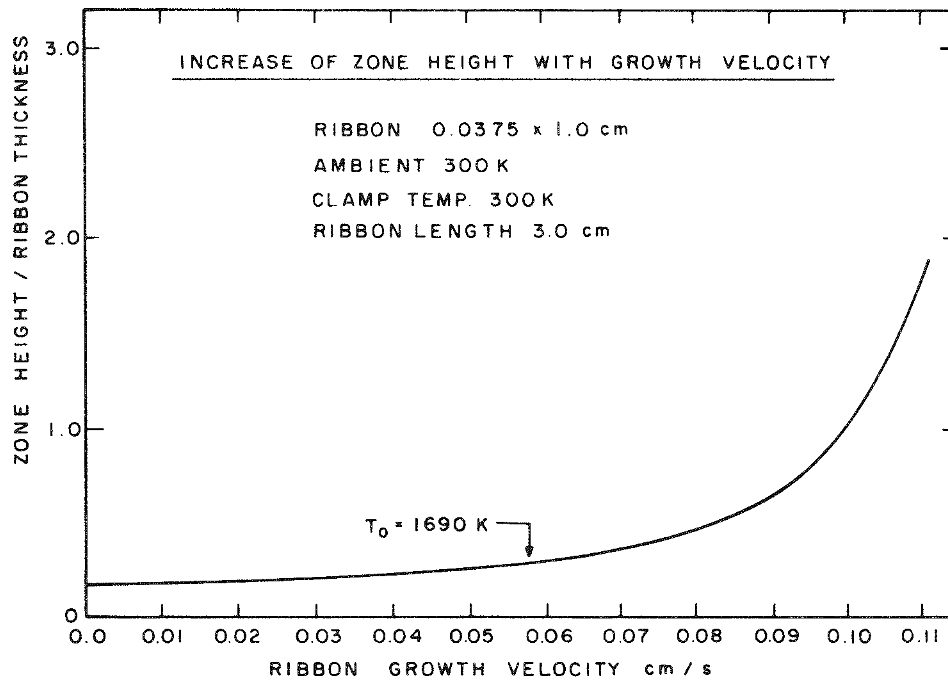

Figure 10. Zone height (normalized to ribbon thickness) as a function of growth velocity taken from the data shown in Fig. 9.

TABLE 2. INFLUENCE OF GROWTH VELOCITY ON THE THERMAL CHARACTERISTICS OF GROWING RIBBON FOR 300 K AMBIENT AND 1690 K DIE TEMPERATURE

Die Temp T_D (K)	Ambient Temp (K)	Growth Velocity V (cm/s)	(in./min)	Zone Height H (cm)	$\frac{H}{t}$	Latent Heat Input Q_c (W)	Net Convective Input P_c (W)	Power Conducted From Die P_D (W)	Total Power Dissipated (W)	Mode of Power Dissipation %			
										Radiation	Convection	Conduction	Convective Transport
1690	300	0.0	0.0	0.006	0.17	0.0	0.0	19.5	19.0	80	13	7	0
1690	300	0.03	0.71	0.007	0.18	4.66	3.17	13.8	21.7	76	12	9	3
1690	300	0.06	1.42	0.012	0.31	9.31	6.32	8.46	24.9	73	11	10	6
1690	300	0.10	2.36	0.037	0.99	15.5	10.52	2.76	30.4	71	10	12	7
1690	300	0.11	2.60	0.067	1.79	17.1	11.6	2.88	33.3	71	10	12	7

increases steadily, indicating the general elevation of the ribbon temperature profile as was illustrated in Fig. 8.

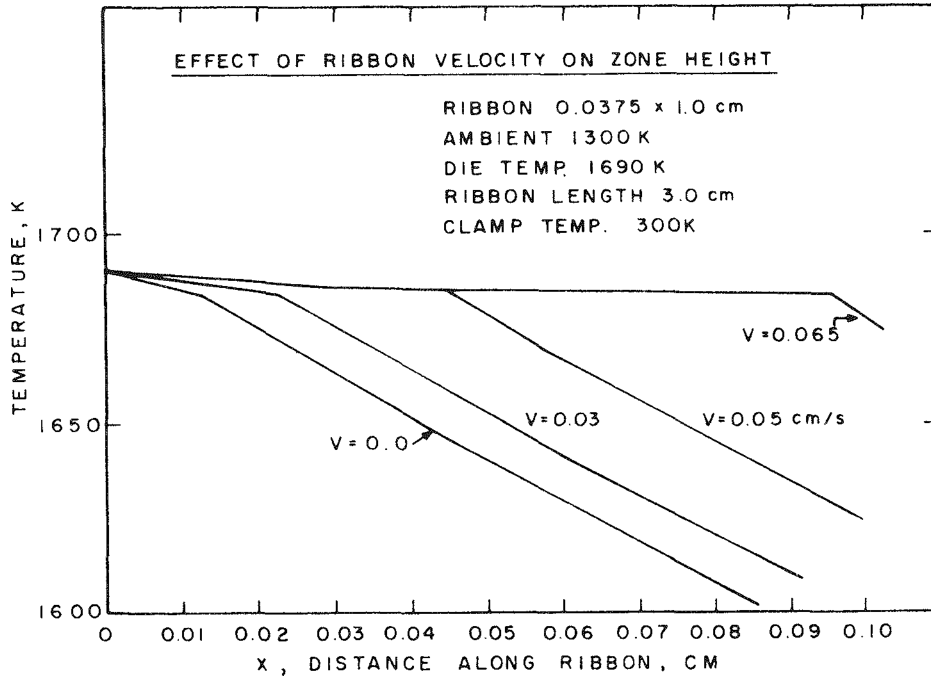

Figure 11. Temperature profile in vicinity of molten zone as a function of growth velocity. Ribbon 0.0375 x 1.0 cm, 3.0 cm long. Die temperature 1690 K, ambient temperature 1300 K.

In Fig. 11 we show the increasing zone height as a function of growth velocity for a 0.0375- x 1.0-cm ribbon, 3.0 cm long, in an ambient of 1300 K with a die temperature of 1690 K. The elevated ambient temperature reduces the power dissipated from the ribbon to the ambient, and, therefore, the temperature gradient at the zone boundary is reduced compared with the ribbon grown in a 300 K ambient. The consequent reduction in the critical growth velocity is apparent, and the zone height is already growing rapidly for velocities in excess of about 0.05 cm/s or 1.18 in./min. At constant growth velocity and ambient conditions, the height of the molten zone may be decreased by reducing the temperature of the die. In Fig. 12 we show the temperature profile for the same ribbon and ambient as in Fig. 11, but with the die temperature reduced to 1685 K. The reduction in zone height at constant velocity is shown most clearly in Fig. 13, and we note that, despite this reduction at subcritical growth velocities, the critical velocity is increased

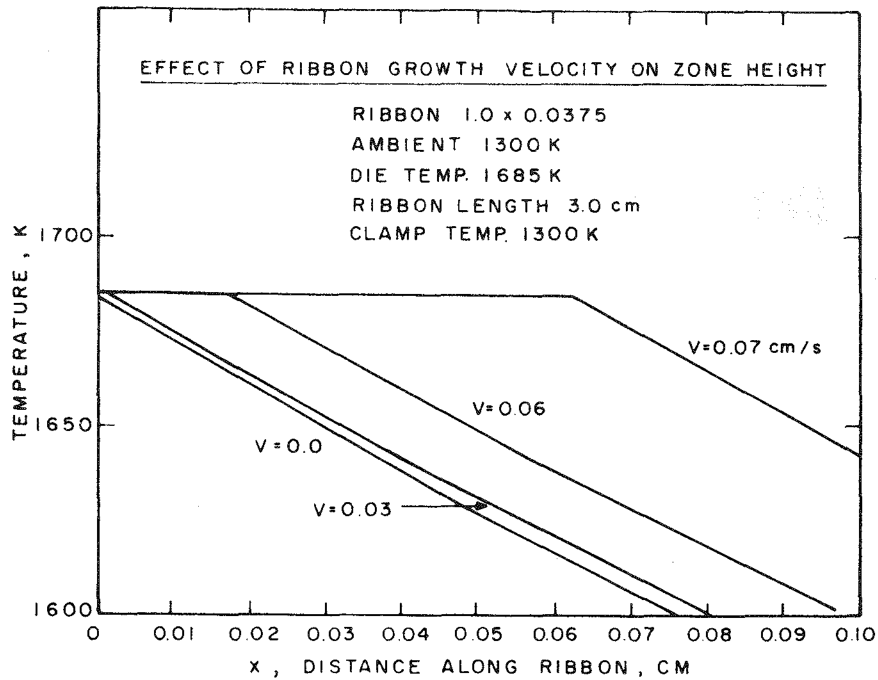

Figure 12. Temperature profile in vicinity of molten zone as a function of growth velocity. Ribbon 0.0375 x 1.0 cm, 3.0 cm long. Die temperature 1685 K, ambient temperature 1300 K.

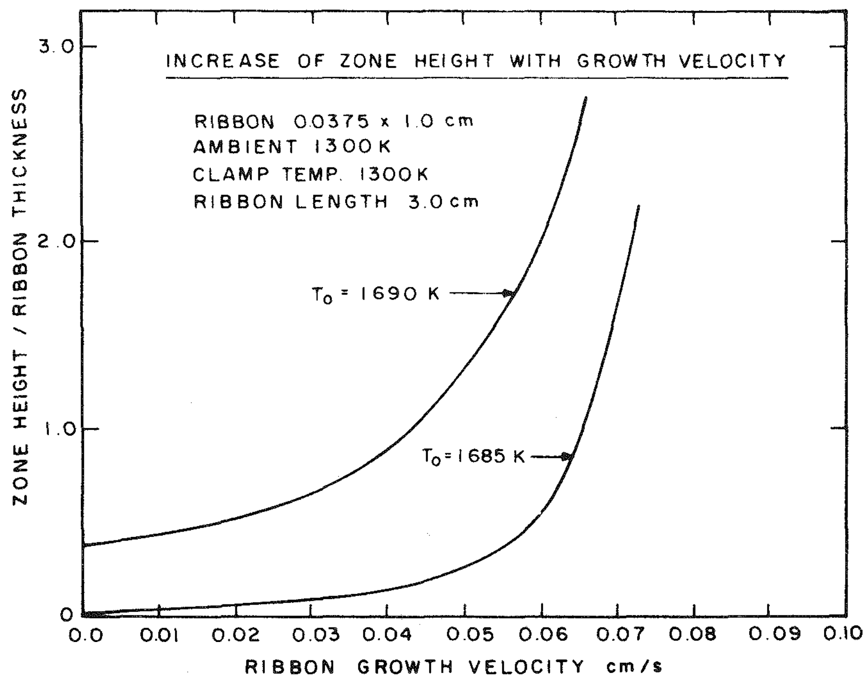

Figure 13. Zone height (normalized to ribbon thickness) as a function of growth velocity taken from data shown in Fig. 11 and Fig. 12.

by perhaps only 20% due to the rapid divergence of the zone height in both cases as the critical velocity is exceeded. Of course, the reduction of the temperature increment of the die aperture above the melting point to only 2 K will increase the practical problems associated with die temperature control and increase the degree to which isothermality is required across the die aperture. Table 3 shows the effect of increasing the growth velocity on the various heat inputs and modes of heat loss from the growing ribbon shown in Figs. 12 and 13. Once again we see that the approach of the growth velocity towards its critical value, where the zone height increases very rapidly, is associated with a reduction of the heat conducted from the die to a small fraction of that observed for a stationary ribbon. In fact, an approximate indication of the critical velocity is obtained by calculating that growth velocity which results in the liberation of latent heat of fusion at a rate just equal to the heat drain on the die to a stationary ribbon, $P_{D,O}$. Of course, $P_{D,O}$ is also equal to the total power dissipated from the stationary ribbon to its ambient and to the clamp.

$$V_{crit} \approx \frac{P_{D,O}}{w\ t\ L} \qquad (4)$$

For a 300 K ambient, $P_{D,O}$ = 19 W and Eq. (4) gives $V_{crit} \approx 0.12$ cm/s, and for the 1300 K ambient with $P_{D,O}$ = 10.5 W, Eq. (4) yields $V_{crit} \approx 0.07$ cm/s in good agreement with the behavior observed in Figs. 10 and 13, respectively.

Equation (4) suggests that some increase in critical growth velocity may be achieved by reducing the ribbon thickness and, thus, the rate of generation of latent heat, although this advantage will be partially offset by the reduced thermal conductance of the thinner ribbon which will result in a reduced $P_{D,O}$. In Fig. 14 we show the temperature profile for a ribbon 1.0 x 0.0187 cm, 3.0 cm long, in an ambient of 300 K for various growth velocities, and the zone height for a given growth velocity is indeed smaller than in the case of the 1.0- x 0.0375-cm ribbon. In Fig. 15, the zone height, normalized to the ribbon thickness, is plotted as a function of growth velocity, and if we, somewhat arbitrarily, take h/t = 2 as the zone stability criterion, then $V_{crit} \approx 0.14$ cm/s compared with $V_{crit} \approx 0.11$ cm/s in the case of the 0.0375-cm-thick ribbon at h/t = 2. Thus we see that the advantage of reduced zone height due to reduced

TABLE 3. INFLUENCE OF GROWTH VELOCITY ON THERMAL CHARACTERISTICS OF A GROWING RIBBON FOR 1300 K AMBIENT WITH DIE TEMPERATURES OF 1690 K AND 1685 K, RESPECTIVELY.

Die Temp T_D (K)	Ambient Temp (K)	Growth Velocity V		Zone Height		Latent Heat Input Q_c (W)	Net Convective Input P_c (W)	Power Conducted From Die P_o (W)	Total Power Dissipated (W)	MOD Mode of Power Dissipation (%)			
		(cm/s)	(in./min)	H (cm)	$\frac{H}{t}$					Radiation	Convection	Conduction	Convective Transport
1690	1300	0.0	0.0	0.014	0.36	0.0	0.0	11.0	10.7	98	2	0	0
1690	1300	0.03	0.71	0.024	0.63	4.66	0.94	6.3	14.5	78	2	0	20
1690	1300	0.05	1.18	0.046	1.23	7.76	1.48	3.95	17.6	70	2	0	28
1690	1300	0.065	1.54	0.096	2.57	10.1	1.94	3.37	21.3	68	2	0	30
1685	1300	0.0	0.0	0.0007	0.02	0.0	0.0	10.4	10.2	98	2	0	0
1685	1300	0.03	0.71	0.0036	0.10	4.66	0.87	5.57	13.7	76	2	0	22
1685	1300	0.06	1.42	0.019	0.50	9.31	1.75	1.12	17.7	65	2	0	33
1685	1300	0.07	1.65	0.064	1.70	10.9	2.03	1.52	20.6	65	2	0	33

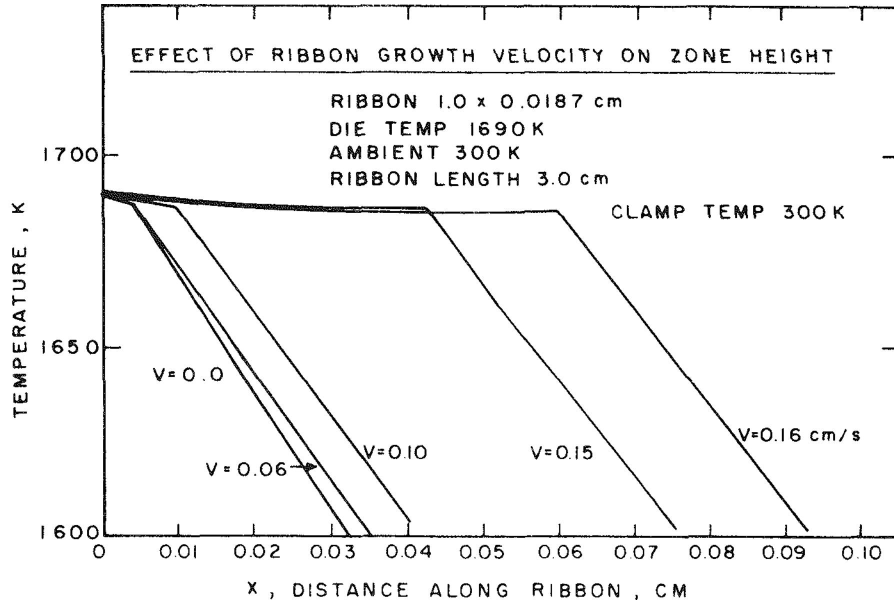

Figure 14. Temperature profile in vicinity of molten zone as a function of growth velocity. Ribbon 0.0187 x 1.0 cm, 3.0 cm long. Die temperature 1690 K, ambient temperature 300 K.

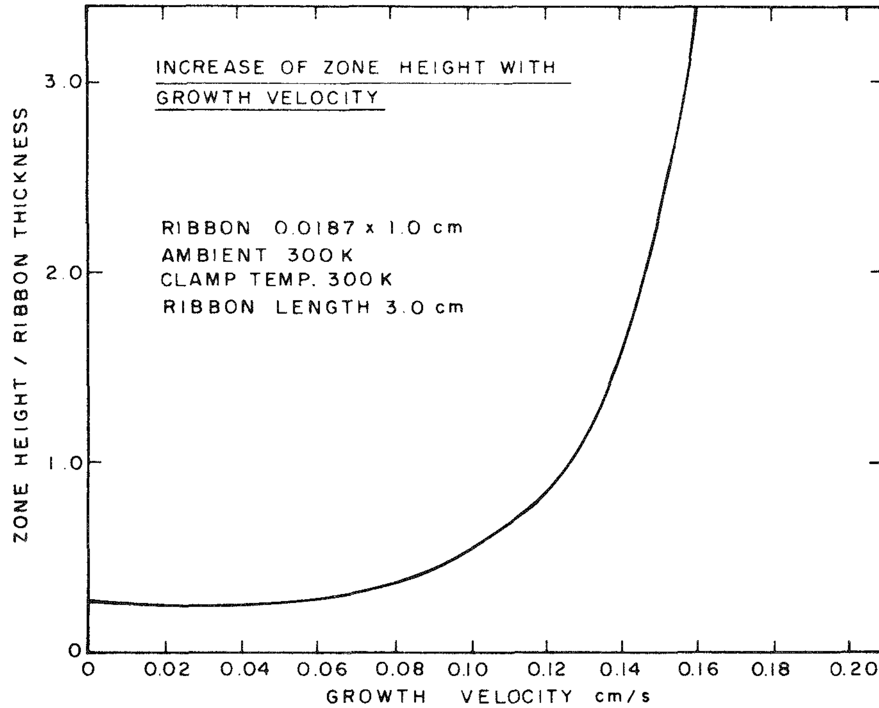

Figure 15. Zone height (normalized to ribbon thickness) as a function of growth velocity taken from data shown in Fig. 14.

generation of latent heat is further offset by the requirement, in absolute terms, of a smaller zone due to the reduced ribbon thickness in order to keep $h/t = 2$. The value of $P_{D,O}$ for the thinner ribbon is 13 W (see Table 4) and Eq. (4) yields 0.17 cm/s. Table 4 again shows that as the critical velocity is approached the heat drain on the die is reduced to a small fraction of $P_{D,O}$.

In summary, our simulation using STEP2C has led to the following conclusions:

(1) The zone height increases with growth velocity, and does so more and more rapidly as a critical growth velocity is approached.

(2) The critical growth velocity is given approximately as that velocity which leads to the generation of latent heat of fusion just equal to the heat conducted from the die by a stationary ribbon under the same thermal conditions.

(3) Highest growth rates are achieved for coolest ambient temperatures and some increase in growth rate is seen when either the die temperature or the ribbon thickness is decreased.

C. COST ESTIMATES OF IST SILICON RIBBON PRODUCTION

We have begun a study of the cost of IST ribbon growth; the study will be developed in terms of the following elements:

(a) Factory parameters: working days/year; shifts/day; hours/shift; labor rates ($/hour); shift premium rates; fringe benefits, expressed as a % of labor for various labor types.

(b) Performance parameters: process yield (%); equipment duty cycle.

(c) Ribbon growth parameters: thickness (cm), width (cm), and growth rate (cm/hour).

(d) Material costs: polysilicon ($/kG); crucibles/dies and seeds ($/day/system).

(e) Direct labor: system requirements for each direct labor type [operator, machine attendant, etc.] (hours/day/system).

TABLE 4. INFLUENCE OF GROWTH VELOCITY ON THERMAL CHARACTERISTICS OF 0.0187 x 1.0-CM GROWING RIBBON FOR 300 K AMBIENT AND 1690 K DIE TEMPERATURE

Die Temp T_D (K)	Ambient Temp (K)	Growth Velocity V (cm/s)	Growth Velocity V (in./min)	Zone Height H (cm)	Zone Height $\frac{H}{t}$	Latent Heat Input Q_L (W)	Net Convective Input P_C (W)	Power Conducted from Die P_D (W)	Total Power Dissipated (W)	Mode of Power Dissipation % Radiation	Convection	Conduction	Convective Transport
1690	300	0.00	0.00	0.005	0.27	0.00	0.00	13.7	13.3	83	14	3	0
1690	300	0.06	1.42	0.005	0.27	4.64	3.15	8.06	10.1	77	14	5	4
1690	300	0.10	2.36	0.010	0.53	7.74	5.26	4.67	18.3	75	13	6	6
1690	300	0.15	3.54	0.043	2.30	11.60	7.90	2.35	22.9	74	12	7	7
1690	300	0.16	3.78	0.063	3.37	12.4	8.39	2.72	24.2	74	11	7	8

(f) Direct expenses ($/day/system): electricity, argon, and furnace parts.

(g) Equipment depreciation expense.

(h) Overhead expenses: indirect labor requirements for each system - supervisory, maintenance, quality control, and engineering support personnel.

(i) Interest on capital investment.

The cost model is depicted in the following diagram:

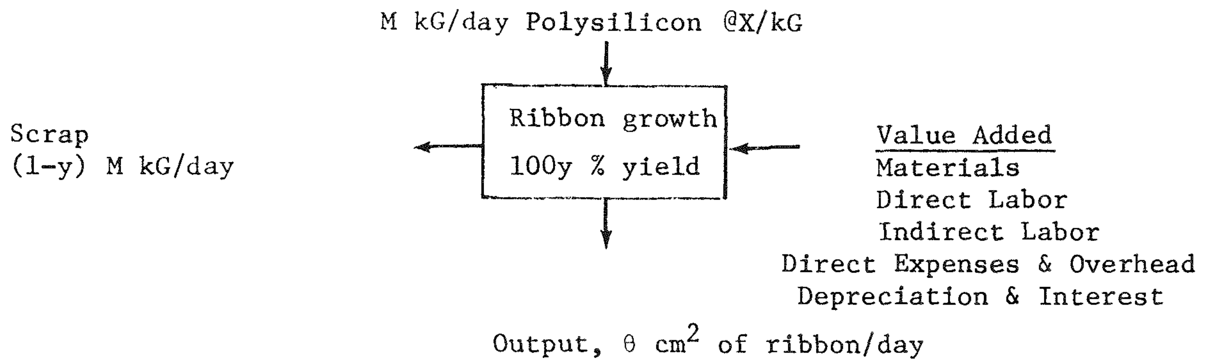

The cost of ribbon, therefore, is as follows:

$$\text{Cost in } \$/\text{cm}^2 = \frac{MX + \text{value added}}{\text{Output, } \theta}$$

where M is the No. of kG/day of polysilicon used and is a function of equipment throughput, duty cycle, ribbon thickness, and yield.

θ is the No. of cm^2/day of ribbon produced and is a function of ribbon growth rate and width and equipment duty cycle.

This cost model and IST ribbon cost estimates will be developed during the next quarter. It is important to note that overhead expenses associated with the process will be individually estimated. The "ratio approach" of representing overhead as a % of direct labor will not be used because these overhead expenses depend on both direct labor and level of production.

An important reason for choosing this type of cost model is that the complete array manufacturing operation can be be represented [6]. This should

6. B. F. Williams, "Automated Array Assembly," Quarterly Report No. 1, ERDA/JPL/954352-76/1, prepared under Contract No. 954352 for Jet Propulsion Laboratory, March 1976.

permit us to use Task 4 (Automated Solar Array Fabrication) results to estimate the cost/watt of array fabrication using IST ribbon. Direct comparisons of starting materials on an area (or even area-efficiency) basis can be misleading due to differences in cell efficiencies, material processing costs, and array packing density factors.

SECTION IV

CONCLUSIONS AND FUTURE PLANS

The thermal gradients with the thermal modifiers such as the L-shaped graphite and pyrolytic graphite plate which have been in use are not satisfactory. Efforts are being made to find a suitable thermal modifier by measuring the horizontal as well as the vertical temperature gradient. With the appropriate thermal modifier, silicon ribbon growth with the applied pressure differential will be pursued. One of the first modifiers to be tested is a pyrolytic graphite plate with regular graphite at the periphery to couple more efficiently to the rf field and, thus, to pump more heat laterally into the PG plate. This configuration has been designed to simulate the satisfactory thermal conditions realized in the earlier rectangular susceptor/flat pyrolytic BN die assembly.

The main conclusions from the application of the computer simulation of the growing ribbon are reported in the final portion of subsection III.C.2. We plan to continue our thermal analysis by examining the zone height variation with growth velocity for more realistic, nonuniform ambient temperatures. We shall also investigate the curvature, $\left(\frac{d^2T}{dx^2}\right)$, of the temperature profile under various ambient conditions as a measure of the residual thermal strain which will be generated in the ribbon.

We plan to take a cost accounting model approach to IST ribbon growth cost estimation so that our cost projections can be combined with Task 4 array fabrication cost estimates. This will provide a cost/watt estimate for solar arrays fabricated using IST ribbon, which we feel is more meaningful than the cost of the silicon substrate alone. Cell efficiency, cell and array processing costs, and array efficiency are important considerations which should not be ignored.

During the next quarter, we plan to develop our cost model and make IST ribbon growth cost estimates. Solar array cost estimates will be made at a later time, after the necessary information becomes available from Task 4.

REFERENCES

1. J. C. Schwartz, T. Surek, and B. Chalmers, J. Electronic Mat. 4, 255 (1975); H. E. Bates, F. H. Cocks, and A. I. Mlavsky, "Thick Film Silicon Growth Techniques," NAS-100/JPL-953365, First Quarterly Progress Report, July 1972.
2. T. F. Ciszek, Mat. Res. Bull. 7, 731 (1972).
3. A. V. Stepanov et al., Bull. Acad. Sci. USSR, Phys. Series 33, 1826 (1969).
4. P. C. Goundry and J. C. Boatman, "Investigation of Single Crystal Si Ribbon," AFAL-TR-66-312, Part I, Sept. 1966, and Part II, Oct. 1967.
5. K. M. Kim et al., "Silicon Sheet Growth by the Inverted Stepanov Technique," Quarterly Report No. 1, ERDA/JPL/954465-76/1, prepared under Contract No. 954465 for Jet Propulsion Laboratory, June 1976.
6. B. F. Williams, "Automated Array Assembly," Quarterly Report No. 1, ERDA/JPL/954352-76/1, prepared under Contract No. 954352 for Jet Propulsion Laboratory, March 1976.

APPENDIX A

NEW TECHNOLOGY

There are no new technology items for this reporting period.

APPENDIX B

PROGRAM PLAN

TASKS	1976 Apr	May	Jun	Jul	Aug	Sep	Oct	Nov	Dec	1977 Jan	Feb	Mar	Apr	May	Jun
THERMAL ANALYSIS	△	—	—	—	—	—	—	—	—	—	—	—	—	—	△
• Theory (Computer Modeling)															
• Experiment															
RIBBON GROWTH	△	—	—	—	—	—	—	—	—	—	—	—	—	—	△
• Modify Model 1	△	—	△												
• Grow 15 ± 5 mil Thick 2 cm Wide Ribbon using SiO_2 Die	△	—	—	—	—	—	—	△							
• Assess 4 mil Thick Ribbon using BN Die				△	—	—	—	—	—	△					
• Develop 10 mil Thick 2 cm Wide Ribbon using SiO_2 Die				△	—	—	—	—	—	—	—	△			
• Optimize Growth for Maximum Velocity using SiO_2 Die								△	—	—	—	—	—	—	△
• Optimize Growth for Crystal Quality Considering Seeding, Die Configuration, Meniscus, SiO_2 Configuration and Other Physical Variables									△	—	—	—	—	—	△
MATERIAL CHARACTERIZATION	△	—	—	—	—	—	—	—	—	—	—	—	—	—	△
MODEL 2 DESIGN & DEVELOPMENT	△	—	—	—	—	—	△								
FINAL REPORT													△	—	△

Month and Duration for Each Task

MILESTONES*

- ← Achieve 400 cm/hr growth rate and 10 mil thick 2 cm wide 30 cm long ribbon; thermal analysis completed
- ← Structural and electrical characterization of 10 mil/2 cm wide ribbon
- ← Growth rate 200 cm/hr
- ← Structural and electrical characterization of 15 ± 5 mil/ 2 cm ribbon
- ← Thermal analysis (experimental measurement); growth rate 100 cm/hr
- ← Optimum s-ℓ interface/meniscus height relationship
- ← Adjust thermal gradient for 2 cm wide ribbon
- ← Assess 10 mil thick ribbon with BN die; complete satisfactory seeding procedure
- ← Grow 20 mil thick, 1 cm wide ribbon; growth rate 50 cm/hr
- ← Die changes to optimize thermal gradient
- ← Thermal analysis (computer modeling)
- ← Preliminary design review of Model 2
- ← Complete the configuration for mechanical support of the SiO_2 die and crucible

*These are the supplemental and/or intermediate goals to the tasks on the left.

APPENDIX C

MANHOURS AND COSTS

At the end of the first quarterly period, manhours were 1289 and cost plus fixed fee was $42,971. Manhours for July and August were 674 and cost plus fee was $24,102. Manhours and cost for September are estimated to be 210 and $7,988, respectively. Second quarter manhours are estimated to be 884 and cost plus fixed fee to be $32,090. Cumulative manhours and cost plus fixed fee are estimated to be 2173 and $75,127, respectively. See Figs. C-1 and C-2.

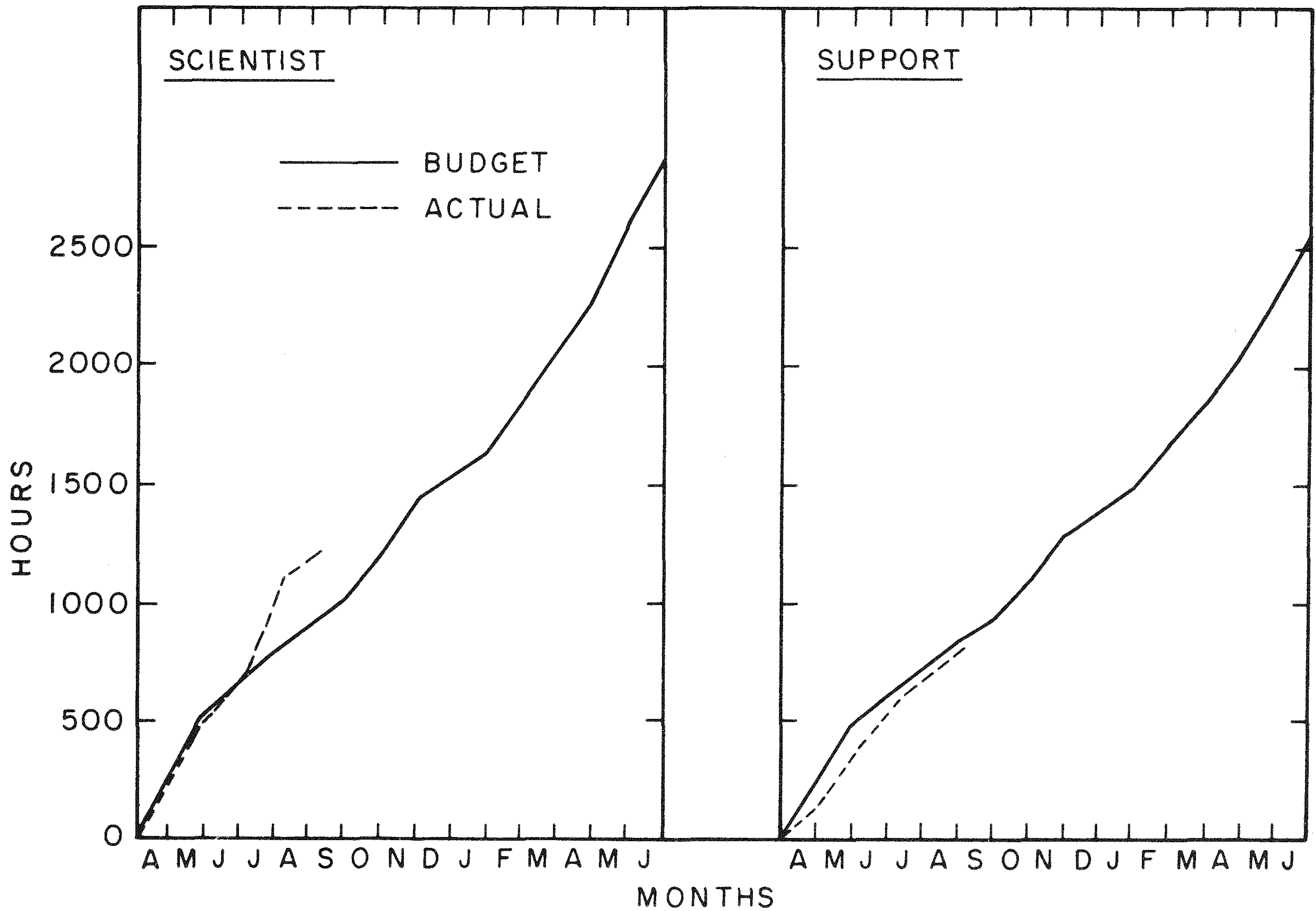

Figure C-1. Manhour chart.

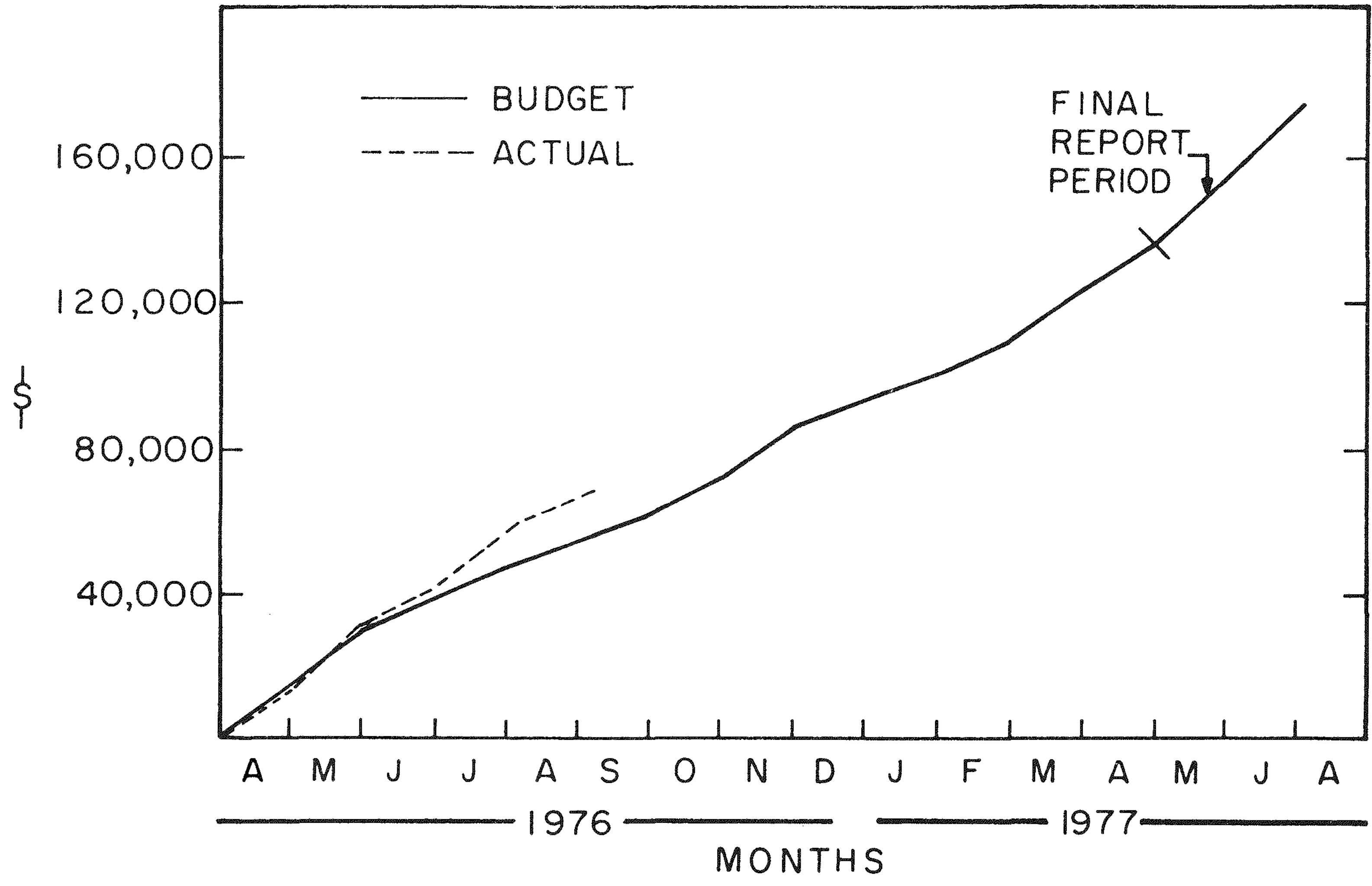

Figure C-2. Cost chart.